Effect of N interstitial complexes on the electronic properties of $GaAs_{1-x}N_x$ alloys from first principles

José D. Querales-Flores,[1,2,3,*] Cecilia I. Ventura,[2,4] and Javier D. Fuhr[2,3]
[1]*Tyndall National Institute, Lee Maltings, Dyke Parade, Cork T12 R5CP, Ireland*
[2]*Centro Atómico Bariloche–CNEA and CONICET, Avenida Bustillo Km. 9.5, 8400 Bariloche, Argentina*
[3]*Instituto Balseiro, Universidad Nacional de Cuyo and CNEA, 8400 Bariloche, Argentina*
[4]*Universidad Nacional de Río Negro, 8400 Bariloche, Argentina*

(Received 6 November 2018; revised manuscript received 21 December 2018; published 19 February 2019)

Although several approaches have been used in the past to investigate the impact of nitrogen (N) on the electronic structure of $GaAs_{1-x}N_x$ alloys, there is no agreement between theory and experiments about the importance of the different N interstitial defects in these alloys, and their nature is still unknown. Here we analyze the impact of five different N defects on the electronic structure of $GaAs_{1-x}N_x$ alloys, using density-functional methods: we calculate electronic states, formation energies, and charge transition levels. The studied defects include N_{As}, As_{Ga}, As_{Ga}-N_{As} substitutional defects and $(N\text{-}N)_{As}$, $(N\text{-}As)_{As}$ split-interstitial complex defects. Our calculated defect formation energies agree with those reported by Zhang *et al.* [Phys. Rev. Lett. **86**, 1789 (2001)], who predicted these defects. Among the interstitial defects, we found that $(N\text{-}As)_{As}$ emerges as the lowest energy configuration in comparison with $(N\text{-}N)_{As}$, in agreement with recent experiments [Jen *et al.*, Appl. Phys. Lett. **107**, 221904 (2015)]. We also calculated the levels induced in the electronic structure due to each of these defects: defect states may occur as deep levels in the gap, shallow levels close to the band edges, and as levels resonant with bulk states. We find that the largest changes in the band structure are produced by an isolated N atom in GaAs, which is resonant with the conduction band, exhibiting a strong hybridization between N and GaAs states. Deeper levels in the band gap are obtained with $(N\text{-}N)_{As}$ split-interstitial defects. Our results confirm the formation of highly localized states around the N sites, which is convenient for photovoltaics and photoluminescence applications.

DOI: 10.1103/PhysRevMaterials.3.024602

I. INTRODUCTION

Defects, whether intentional or not, have a dominant impact in both electrical and optical properties of semiconductor alloys [1]. The rich variety of defects along with their technological importance guarantee interest in their computational research. III-N-V semiconductors, in particular GaAsN alloys, can be lattice matched to substrates such as GaAs, Ge, and Si, with a range of direct gaps that are complementary to those of other III-V semiconductors [1–5]. There are many applications for these alloys including the next generation of high-efficiency multijunction solar cells, high-performance electronic devices, and long-wavelength light emitters and detectors.

Intrinsic point defects have been identified in GaAsN as As_{Ga} antisites [6], N interstitials [7,8], and Ga vacancies [9]. Experimental and theoretical works have suggested that the majority of N atoms incorporated to GaAs could be expected to go to isoelectronic substitutional As sites [10,11]. However, Zhang and Wei [10] suggested that a significant fraction of N atoms incorporate nonsubstitutionally as split interstitials: $(N\text{-}N)_{As}$ or $(N\text{-}As)_{As}$. For substitutional N atoms on As sites, it is energetically more favorable to be somewhat apart from each other and thus the equilibrium thermodynamics does not favor the formation of nitrogen pairs [12]. The reason for this is that although the total energy can be lower when two defects share their surrounding shear fields, two N atoms being too near to each other causes larger structural changes in the host crystal than being somewhat more apart. In dilute N containing GaAs, it has been reported that the presence of (N_{As}-N_{As}) substitutional pairs is negligible [13]. Direct measurements of the fraction of N incorporated interstitially in GaAs via nuclear reaction analysis (NRA) have been reported by several groups [7,8,14–16]. More recently, Jen *et al.* [16] reported a comparison between Rutherford backscattering spectroscopy and NRA with Monte Carlo molecular dynamics simulations, in order to distinguish $(N\text{-}N)_{As}$, $(N\text{-}As)_{As}$, and (As_{Ga}-N_{As}) complexes in GaAsN alloys. The results suggested that $(N\text{-}As)_{As}$ is the dominant interstitial complex in dilute GaAsN, in contrast to previous electronic structure calculations, based on density functional theory (DFT), which predicted $(N\text{-}N)_{As}$ to be the most energetically favorable configuration [11,17]. In 2017, Occena *et al.* [18] examined the influence of the flux on bismuth and nitrogen incorporation during molecular beam epitaxy of $GaAs_{1-x-y}N_xBi_y$ alloys, and observed an enhancement in total N incorporation via the formation of additional $(N\text{-}As)_{As}$. It is worth mentioning that the presence of split interstitials have been reported in other III-V semiconductors, for instance (N-As) bonding defects in (Ga,In)(N,As)/Ga(N,As) heterostructures [19] and TlInGaAsN alloys [20] and (Sb-N) split interstitials in

*jose.querales@tyndall.ie

(InGa)(AsSbN)/GaAs quantum wells [21] and $InSb_{1-x}N_x$ alloys [22,23].

In Ref. [12] the impact of $(N\text{-}N)_{As}$ interstitial, N_{As}-N_{As} substitutional pairs, and N substitutional on the electronic properties of GaAsN alloys was studied within the hybrid functional scheme (HSE06). However, the relationship between N incorporation as $(N\text{-}As)_{As}$ and $(As_{Ga}\text{-}N_{As})$ has not been reported yet. Nevertheless, several theoretical approaches have been used in order to investigate the impact of N on the electronic structure of $GaAs_{1-x}N_x$ alloys. For instance, first-principles [11,17,24,25], empirical pseudopotential [26,27], and sp^3s^* tight-binding [28–30] calculations of supercells have been performed, giving valuable insight on the microscopic mechanisms of formation of band-edge states in $GaAs_{1-x}N_x$. The band structure of $GaAs_{1-x}N_x$ substitutional alloys was studied in the framework of DFT within the hybrid functional scheme (HSE06) [12], and it was found that the trends in the band-gap reduction in these alloys result mainly from the positions of the N-induced states with respect to the bottom of the bulk conduction bands. Reference [31] demonstrated the accuracy of the HSE06 hybrid functional for computing the band offsets of semiconductor alloy heterostructures, including GaAs. The formation energies and transition levels of a set of interstitial-type defects of N in GaAs have been determined by DFT calculations, in local density approximation (LDA) [17], and generalized gradient approximation (GGA) [11]. Nevertheless, for N-N split interstitial defects, differences were observed between the band-gap transition levels calculated with LDA and GGA approximations [11,17].

It is known that point-defect formation energies calculated within the framework of density functional theory often depend on the choice of the exchange and correlation (*xc*) functional. Regarding that, Freysoldt, Lange, and Neugebauer [32] showed that variations between the LDA, GGA, and hybrid functionals emerge from differences in the position of the bulk valence-band maximum, as well as in the reference energies for the chemical potential obtained with distinct *xc* functionals. Freysoldt *et al.* [32] used a band-alignment strategy, based on aligning a benchmark defect level between GGA and hybrid functional calculations; they also included changes to reference energies for chemical potentials between functionals.

In this work, we determine formation energies and charge transition levels for a large set of N defects in GaAs using a supercell approach for defects calculations in GGA approximation and hybrid functionals calculations for the reference energies for the chemical potential, adopting the framework recently proposed in Ref. [32]. In particular, we investigate the case of single-atom substitutional defects N_{As} and As_{Ga}. We also consider complex defects such as As_{Ga}-N_{As}, in which the N_{As} defect binds to one As_{Ga} antisite, and split interstitials $(N\text{-}N)_{As}$ and $(N\text{-}As)_{As}$, in which a dimer of N-N or N-As is located in an As site.[1] Our results suggest that $(N\text{-}As)_{As}$ is the dominant split interstitial in dilute GaAsN, in agreement with recent experimental results [16,18]. We also calculated the induced levels in the electronic structure due to each of these defects. Depending on the defect, these states occur as deep levels in the band gap, as shallow levels very close to the band edges, as well as levels in-between the bulk states. We find that the most prominent of these levels is due to an isolated N atom in GaAs, which is resonant with the conduction band, exhibiting a strong hybridization between N and GaAs states. Deeper levels in the energy gap have been found for N pairs. These results confirm the formation of highly localized electronic states around the nitrogen sites, which is favorable for applications [5,34,35]. In addition, our results for the effect of the substitutional N_{As} defect on the electronic structure of GaAs agree very well with those given by the well-known band anticrossing model [36], therefore providing further support to it.

This paper is organized as follows. In Sec. II, we describe our theoretical approach based on DFT calculations. In particular, we discuss the method we adopted to calculate the defect formation energies by combining GGA and hybrid functionals calculations. The results of our calculations are given in Sec. III, where they are compared to previous theoretical and experimental results. In Sec. IV, the conclusions are summarized.

II. THEORETICAL APPROACH

The most relevant thermodynamic quantity characterizing a point defect X in charge state q is its formation energy, as comprehensively reviewed by Van de Walle, Neugebauer, *et al.* in Refs. [37,38], given by

$$E_f(X^q) = E_t[X^q] - E_t[\text{Bulk}] - \sum_i n_i\mu_i + q[\mu_e + \Delta V], \tag{1}$$

which depends on the chemical potentials μ_i of atoms that have been added ($n_i > 0$) or removed ($n_i < 0$) and the chemical potential for electrons $\mu_e = E_F + E_{\text{VBM}}$, E_F and E_{VBM} being the Fermi level and the valence band maximum respectively. $E_t[X^q]$ and $E_t[\text{Bulk}]$ are the calculated total energies of the defect X (in charge state q) and bulk respectively. The chemical potentials μ_i of the n_i added or removed atoms allow us to take into account the growth conditions. ΔV corresponds to a correction for the finite size of charged supercells, in order to align the electrostatic potentials [17]. In our present work, ΔV was calculated as the difference of the electrostatic potential in the host and defects supercells far from the defect [39].

We have determined the formation energies and transition levels of nitrogen defects in GaAs, with spin-polarized DFT total energy calculations. All defect configurations are obtained through full structural relaxation carried out within

[1]The effects of hydrogen on the electronic properties of dilute GaAsN Alloys have been studied in Ref. [33], where the results showed that nitrogen alloying qualitatively alters the electronic behavior of monoatomic hydrogen to become only a donor, despite the fact that in GaAs or GaN hydrogen is amphoteric, existing in either donor or acceptor states. At higher hydrogen concentrations, it is energetically more favorable to form self-compensated, charge neutral H*2N complexes. The formation of these complexes completely eliminates the band-gap reduction caused by nitrogen.

a DFT framework in which the exchange-correlation energy is described through the semilocal approximation proposed by Perdew, Burke, and Ernzerhof (PBE) [40,41]. To obtain the chemical potential of atoms, μ_i in Eq. (1), we performed calculations using the screened hybrid functional of Heyd, Scuseria, and Ernzerhof (HSE) [42,43]. We used the VASP (Vienna Ab-initio Simulation Package) code [44] with the projector augmented wave (PAW). We used a plane-basis set defined by a kinetic energy cutoff of 400 eV and the gallium 3*d* states were treated as valence states. We performed calculations using 64- and 65-atom supercells with a $3 \times 3 \times 3$ k-point set generated using the Monkhorst-Pack method. We study the convergence of the total energy with respect to the $\vec{k}$-point grid: we got converged results for a sampling of $3 \times 3 \times 3$. We have used a supercell size as typically used in previous studies [12,17]. In Ref. [17], 64- and 216-atom supercells gave similar formation energies (less than 70 meV) and transition levels showing good convergence as a function of the supercell size.

For neutral defects the hybrid functional calculations were incorporated as a correction for the chemical potentials of the individual species in Eq. (1), in our case Ga, As, and N. This is shown in Ref. [32] for Ga and As. For calculating corrections we require that the corrections reproduce the HSE enthalpy of formation ($\Delta H^{f,\mathrm{HSE}}$) of N_2, GaN, and GaAs, by taking HSE as the best available theory reference. We obtained PBE corrections for Ga, As, and N: +0.075, −0.689, and +0.68 eV, respectively. As discussed in Ref. [32], when appropriate corrections are applied, the standard local and semilocal functionals can be used to screen for relevant defect configurations before using the computationally more demanding HSE hybrid functionals or *GW* approximation.

On the other hand, for charged defects the chemical potentials for electrons is needed. We corrected the position of the bulk valence band entering Eq. (1) as reference for the Fermi level [32]. Reference [32] shows that this approach corrects the known weakness of a functional in describing the extended host states, while leaving the description of the localized defect states unaltered. This is appropriate for defects that possess well-localized defect states within the band gap.

We fully relax the unit cell to obtain the lattice constants for GaAs of 5.7497 Å, consistent with earlier reports [45]. The atomic positions are relaxed until the Hellmann-Feynman force acting on each atom is reduced down to less than 1.0 meV/Å.

The unfolding of the supercell bandstructure has been performed using the BANDUP code [46,47]. In order to have a good description of the band gaps, for the calculation of electronic properties (density of states and band structure) we used the modified Becke-Johnson (mBJ) exchange potential in combination with LDA correlation [48,49], and GGA structural parameters.

III. RESULTS AND DISCUSSION

Here, we will present structural and electronic structure results obtained using our approach described in Sec. II, in four subsections. As mentioned in the Introduction, the substitutional N_{As} defect has been extensively studied in comparison with those interstitials ones. In our analysis of the electronic structure of GaAsN alloys, we will always include our own results for N_{As} as a validation of the approach we used. In Sec. III A, we will discuss and compare our results for the structural properties for the N defects studied, with recent theoretical values, when available. In Sec. III C, we show our results for the total and projected densities of states, in order to identify the N-induced electron states around the gap of GaAs. In Sec. III B we analyze the formation energies for charged defects, for all studied N configurations as a function of Fermi energy. In Sec. III D, we will describe the unfolded band structure for each N defect in connection with the results first presented in Sec. III C.

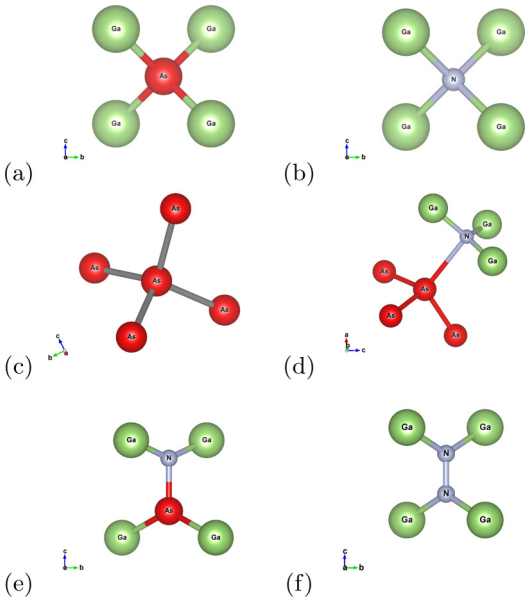

FIG. 1. Configurations of native defects in $GaAs_{1-x}N_x$. (a) Crystalline GaAs, (b) single N atom located in an arsenic site, N_{As}, (c) single arsenic atom located in a gallium site, As_{Ga}, (d) N_{As} defect binds to one As_{Ga} antisite, As_{Ga}-N_{As}, (e) N-As pair in an arsenic site, $(N\text{-}As)_{As}$, and (f) N-N dimer in an arsenic site, $(N\text{-}N)_{As}$. The figures were generated using VESTA software [50].

A. Structure of the studied defects

Figure 1 shows the structure of an As atom and its neighbors in GaAs [Fig. 1(a)], along with the five complex defects studied in this work [Figs. 1(b)–1(e)]. When a N atom is incorporated in an As substitutional lattice site, the following bonds are formed with respective bond lengths: 2.1119 Å for N-Ga and 2.4902 Å for As-Ga. We found that N incorporates in the split interstitial (N-N), in which two N atoms share a substitutional lattice site with a strong bond between them: 1.3349 Å is the N-N bond length and 2.0220 Å the N-Ga one. The N-N bond-length results are consistent with previous LDA studies, i.e., 1.34 Å [17] and 1.33 Å [11], while the value obtained for the N-Ga bond length is slightly larger than 1.95 Å reported in Ref. [17] for LDA.

When N incorporates in the other split interstitial configuration, in which a dimer with N-As atoms occupies a substitutional lattice site, we find 1.7998 Å for N-As bond length (LDA: 1.79 Å [17]), 2.4351 Å for As-Ga bonds (LDA:

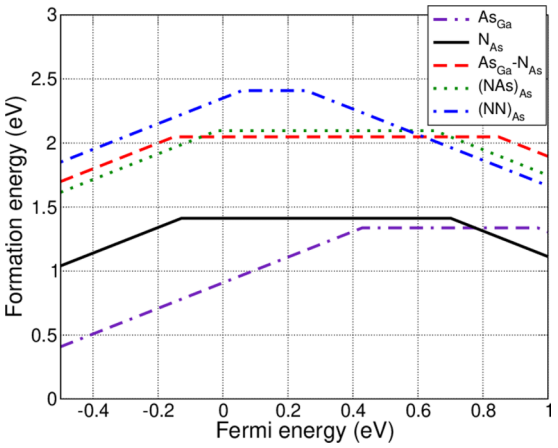

FIG. 2. Formation energies vs Fermi level for substitutional, interstitial, and antisite defects in $GaAs_{1-x}N_x$, calculated with a GGA and HSE hybrid functionals corrections, as proposed by Freysoldt *et al.* in Ref. [32]. All sets of formation energies include finite-size corrections [see last term in Eq. (1)]. The Fermi-level range is extended beyond the band maxima. In all cases, As-rich conditions are chosen, i.e., $\mu_N = \mu_{N_2/2}$. The lattice constant was taken as the DFT-GGA one, mentioned in Sec. II.

2.38 Å [17]), and 1.9298 Å for N-Ga bonds (LDA: 1.88 Å [17]). For substitutional As_{Ga}, we find that 2.6085 Å As-As and 4.0893 Å As-Ga bonds are formed.

B. Thermodynamic transition levels of N defects in $GaAs_{1-x}N_x$

According to Eq. (1) the higher the Fermi level is, the more energy is gained by moving the electron from the reservoir into the defect. That is, the formation energy of a negatively charged defect gets lower at higher values of the Fermi level, and vice versa for the positively charged defects. If the defect has the lowest formation energy in the negative charge state, then a neutral defect would like to receive an electron from the electron reservoir, so that it behaves like an acceptor. In a similar way, if a neutral defect likes to donate an electron to the electron reservoir, it becomes positively charged and this can be related with a donor. When the formation energies of all the possible charge states are calculated, the charge state yielding the lowest formation energy depends on the Fermi level. Consequently, there will be a value of E_F where the formation energy is the same for two charge states, which is usually denoted as ionization level, hereafter denoted as $\epsilon(q_1/q_2)$. This level is the same as the energy required to promote an electron from the valence band into the defect for acceptor levels or demoting an electron from the defect to the valence band for donor levels. The atomic structures of the defects in charge states q_1 and q_2 can be different. If the atomic relaxation occurs during the ionization process, it is called thermodynamic transition. If not, it is called an optical transition. Formation energies for thermodynamic transitions of native defects in $GaAs_{1-x}N_x$ calculated with GGA (PBE) and HSE are presented in Fig. 2. As-rich conditions in Eq. (1) have been chosen, i.e., $\mu_N = \mu_{N_2/2}$. In our calculation, for each charged defect configuration a fully structural relaxation was done.

Figure 2 shows the calculated formation energies for all studied defects as a function of Fermi energy. In principle the Fermi level ranges from the VBM up to conduction band minimum. We chose the range of Fermi level to be ∼1 eV above the VBM based on the location of the defects states identified (it will be discussed in Sec. III C). In the following we describe the main results.

N-N split interstitials: N gives rise to two transition levels within the band gap of $GaAs_{1-x}N_x$. Concretely, the transition from the neutral to +1 charge state (0/+1) happens when the Fermi energy is 0.058 eV above the valence band maximum, while the transition from the neutral to −1 charge state (0/−1) occurs at a Fermi energy equal to 0.256 eV. This defect was found to be stable in positively charged states when the Fermi level is in the lower part of the band gap, stable in the neutrally charged state for a limited number of values of the Fermi level in the gap, and becoming negatively charged at higher Fermi levels.

N-As split interstitials: Only one transition level within the band gap of $GaAs_{1-x}N_x$ is found, from neutral to −1 charge state (0/−1) at the Fermi energy 0.651 eV. For most Fermi energy values the interstitial defect with the lowest energy is $(N\text{-}As)_{As}$.

N substitutional: We find one transition level in the band gap for the substitutional N_{As} and As_{Ga}-N_{As} antisite defects: the transition (0/−1) happens for the N_{As} and As_{Ga}-N_{As} defects at Fermi energies of 0.7 and 0.848 eV above VBM, respectively. It is worth mentioning that in previous LDA and GGA calculations in Refs. [11,17] no such charged states transitions for N_{As} had been found. However, from LDA calculations reported in Ref. [51] the 0/−1 transition was predicted to occur at Fermi level ∼0.82 eV above the maximum of the valence band. We did not find experimental studies on it.

As_{Ga} substitutional: We find two transition levels in the band gap: (+1/0) happens for the defect at Fermi energy 0.428 and (0/−1) at 0.969 eV above VBM, respectively. The occupation of the Ga site by As leads to insignificant lattice distortions, involving the formation of defects with the lowest formation energy.

The calculated charge transition levels, Fermi energy for neutral defects, and formation energies are listed in Table I together with the results of previous first-principles calculations, for comparison.

C. Electron density of states

The GaAs direct band gap E_g obtained with GGA is much smaller with respect to the experimentally reported one (∼1.52 eV [31,52]): using the GGA optimized lattice parameter, $E_g = 0.18$ eV, which increases to 0.56 eV if the experimental lattice parameter is used in the calculation. For a better description of the electronic structure of bulk GaAs and its defects, we used the mBJ exchange potential in combination with LDA correlation [48,49], which is known to yield band gaps with an accuracy similar to hybrid functional or *GW* methods. With this approximation the calculated bulk GaAs band gap is ∼1.64 eV, much closer to the experimental value.

In Fig. 3 we show the calculated total and projected densities of states of bulk GaAs and of the five defects

TABLE I. Charge transition levels ($\epsilon_{q/q'}$), Fermi energy for neutral defects (E_F^0), and formation energies (E_f) calculated at the PBE level, and including hybrid functional corrections for electron and chemical reservoirs and Ga 3*d* states in the valence band, for the most relevant defects. For comparison, we also show corresponding formation energies calculated in Refs. [11,17,45,51]. E_F^0 for GaAs: 2.717 eV.

Defect	E_F^0 (eV)	E_f (eV)	$\epsilon_{+1/0}$ (eV)	$\epsilon_{0/-1}$ (eV)
As_{Ga}	3.280	1.337 (1.33 [45])	0.428	0.969
N_{As}	2.633	1.406 (1.087 [11])	−0.128	0.7 (0.82 [51])
As_{Ga}-N_{As}	2.635	2.048	−0.151	0.848
$(N\text{-}As)_{As}$	3.118	2.178 (2 [17])	−0.018	0.651 (0.29 [17])
$(N\text{-}N)_{As}$	2.730	2.462 (2.754 [11])	0.058 (0.2 [11])	0.256 (0.12 [17], 0.3 [11])

in $GaAs_{1-x}N_x$ considered in this study. The projected density of states includes the contribution from the first neighbors around each defect configuration. The Fermi levels in the density of states in Fig. 3 were aligned with respect to the position of a core level, and are shown with respect to the Fermi level of bulk GaAs. From the density of states we can get information about the carrier type induced by each kind of defects. In particular, we find that, for the defects As_{Ga}, $(N\text{-}As)_{As}$, $(N\text{-}N)_{As}$, As_{Ga}-N_{As}, localized states can be identified as narrow peaks within the bulk GaAs band gap (indicated by vertical dotted lines in Fig. 3). The localized character of the $(N\text{-}N)_{As}$ dimers was suggested from first-principles pseudopotential method studies in Ref. [53]. Meanwhile, for substitutional N_{As} no localized states within the band gap can be identified, indicating a strong hybridization between N states and GaAs states at the edge of the valence and/or conduction bands.

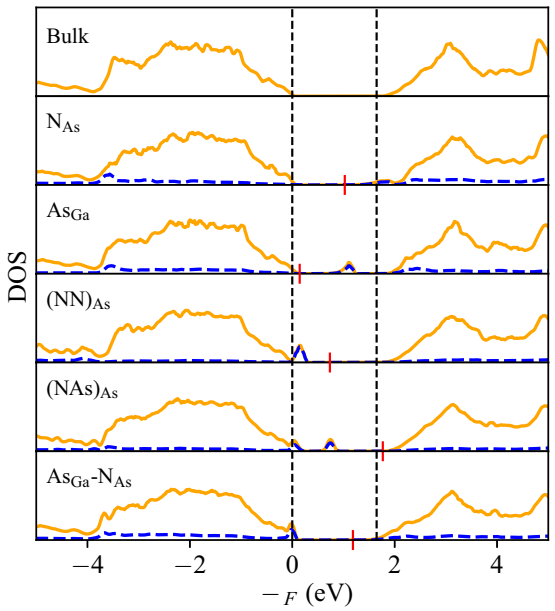

FIG. 3. Total density of states (DOS) for bulk GaAs and the five defect configurations. Vertical lines along the whole figure indicate the calculated band gap for pure GaAs. Full lines represent the DOS and dashed lines the projected DOS on each defect including its first neighbors. The PDOS corresponding to N_{As} was multiplied by a factor of 10. The small vertical full lines indicate the Fermi level for each defect configuration.

D. Unfolding of the supercell band structures

To get meaningful information from the massive number of bands of a GaAs with N defect systems, we employ the technique of band unfolding by using the recently released BANDUP code [46,47]. With this technique we can obtain the unfolding of the bands in the Brillouin zone (BZ) of the large supercell back into the BZ of the primitive unit cell of GaAs. As done for the density of states, the Fermi levels in the density of states in Figs. 4 were aligned with respect to the position of a core level, and are shown with respect to the Fermi level of bulk GaAs.

As reference, the unfolded band structure of GaAs close to the band gap is shown in Fig. 4(a). The unfolded band structure for GaAs with each of the different N defects considered in this work, along high-symmetry directions of the primitive cell BZ, are shown in Figs. 4(b)–4(d). As a general result, it can be seen that by introducing N defects in GaAs, some new bands with low Bloch spectral weight appear, mostly close to the band gap. In the following we will discuss in detail the effect of each of the defects on the electronic band structure of GaAs.

In Fig. 4(b), we exhibit the unfolded band structure of GaAs with substitutional N_{As} defects. We observe that N_{As} defects mostly affect the conduction band of GaAs [compare with Fig. 4(a)], causing the formation of quasilocalized electron states associated with the substitutional N atoms, which interact strongly with the GaAs conduction band edge. In particular, the bottom of the conduction band is split, and a second minimum appears at Γ which possesses low spectral weight. Our results are in agreement with previous studies by Shan *et al.* [54], where a simple physical understanding of the dramatic effect of N_{As} defects on the band gap of GaAs was based on the band anticrossing model (BAC), and they showed that the reduction of the energy bandgap could be described by an interaction between the conduction band and a higher-lying set of localized N resonant states [30,55]. In order to validate our results in Fig. 4(b), we compare our obtained band gap with the dilute limit result given by the band anticrossing model in Ref. [36]: the nitrogen concentration in our calculation would correspond to ∼1.56% and the direct gap at is Γ ∼ 1.108 eV, which compares quite well with the value of ∼1.07 eV given by the BAC. Our results also agree with our DOS calculations presented in Fig. 3, where localized N-induced states are not identified when N is incorporated substitutionally.

Figure 4(c) shows the unfolded band structure of GaAs with As_{Ga} substitutional defects. As can be seen in the figure, an electronic state with low dispersion appears in the GaAs gap, closer to the bottom of the conduction band, which is correlated to the sharp peak that can be seen in the corresponding DOS (Fig. 3). In addition, we found that the As_{Ga} defect does

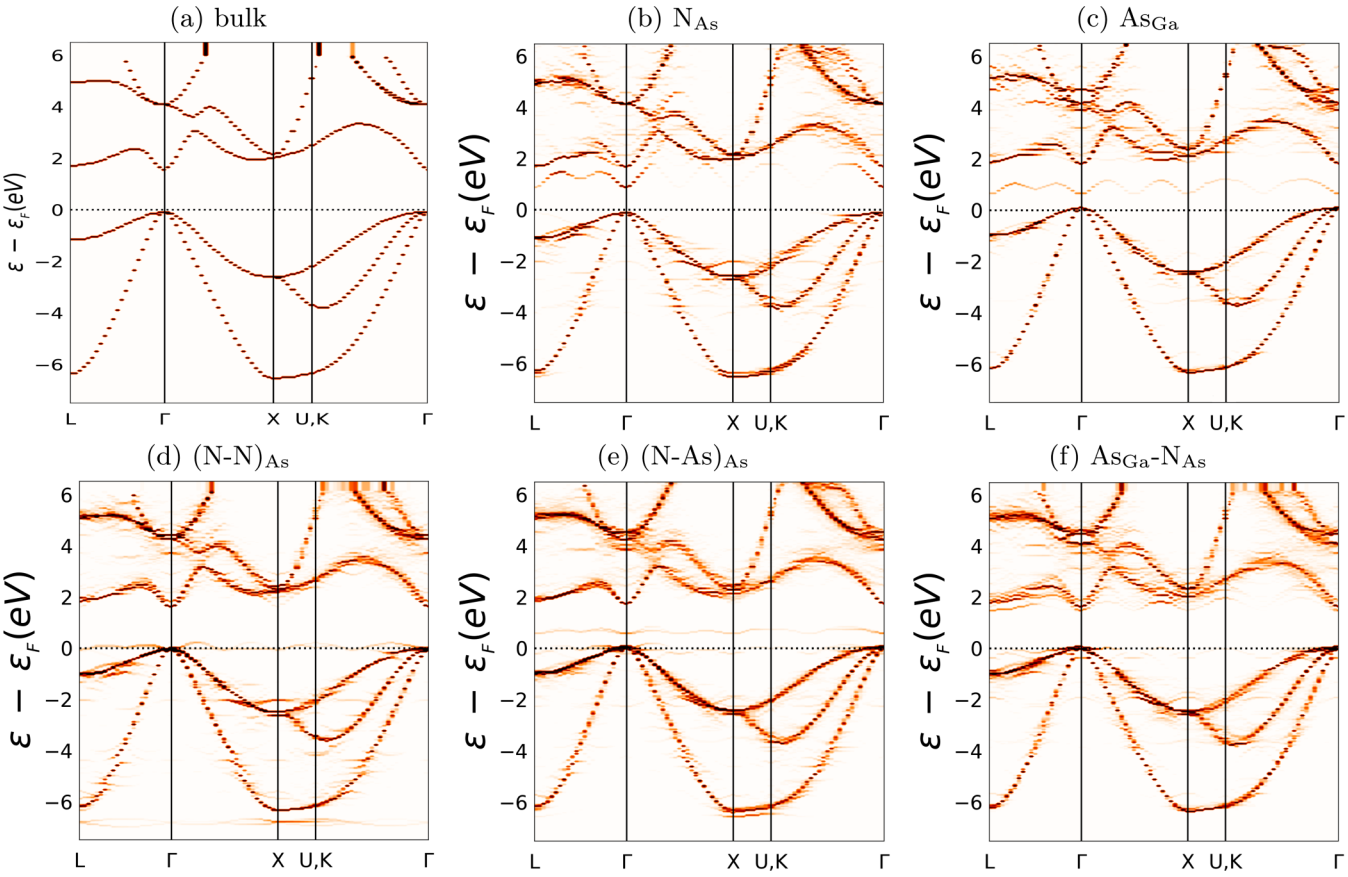

FIG. 4. Effective band structure of bulk GaAs, and the five defect configurations unfolded into a primitive cell of the Brillouin zone using the BANDUP code [46,47]. (a) Bulk GaAs. (b) and (c): N_{As} and As_{Ga} substitutional defects. (d), (e) and (f): $(N\text{-}N)_{As}$, $(N\text{-}As)_{As}$, and $As_{Ga}\text{-}N_{As}$ complex defects respectively. Here, the energy axis is referenced with respect to the Fermi level of bulk GaAs.

not affect much the band edges in GaAs, opposite to the effect of the N_{As} substitutional defect.

In Figs. 4(d) and 4(e), we exhibit the unfolded band structure of GaAs with $(N\text{-}N)_{As}$ and $(N\text{-}As)_{As}$ complex interstitial defects respectively. As can be seen, the bottom of the conduction band is less affected by these defects, in contrast to our findings for the susbtitutional N_{As} defect. In agreement with results previously presented in Fig. 3, $(N\text{-}N)_{As}$ induces quite localized states in the top of the GaAs valence band, which can be seen in the band structure as flat lines with very low spectral weight just below the Fermi level. On the other hand, $(N\text{-}As)_{As}$ induces two localized states, one at the top of the valence band and the other deeper in the GaAs band gap.

Finally, in Fig. 4(f) we exhibit the unfolded band structure of GaAs with the $As_{Ga}\text{-}N_{As}$ defect. We observe that this defect affects both the conduction and valence bands of GaAs, producing first a reduction of the direct gap, as for N_{As}, and second the formation of quasilocalized electron states near the top of the GaAs valence bands. The lines appearing very close to the top of the valence band in Fig. 4(f) can be observed as a sharp peak in the DOS (Fig. 3).

Finally, it is worth mentioning that for devices that rely on good carrier mobility, the process of trapping, detrapping, and scattering by the potential fluctuations reduces mobility and hence performance. So, localized states can result in relatively short carrier lifetimes. Short carrier lifetimes will clearly inhibit the performance of devices such as lasers, which require long carrier lifetimes. However, localization can also be exploited to enhance device performance. In the case of III-nitride materials with high densities of nonradiative centers, exciton localization improves luminescence efficiency by preventing migration of carriers towards the defects. In particular, dilute nitrides could be a good candidate material for avalanche photodetectors [35], where the degradation in electron mobility actually becomes advantageous.

IV. SUMMARY AND CONCLUSIONS

In this work, we have presented calculations of the structural and electronic properties of dilute $GaAs_{1-x}N_x$ alloys using a supercell approach, within the framework of density functional theory and the GGA approximation, using a hybrid functional for the exchange correlation functional. Motivated by the fact that semilocal DFT functionals, like GGA, underestimate the band gap of $GaAs_{1-x}N_x$ alloys, and that this error affects the position of defect levels within the band gap and the values of formation energies, we adopted the Freysoldt *et al.* [32] method, i.e., using formation energies and defect levels as calculated with GGA, but interpreting them within a band gap where the valence band edge has been shifted down and the conduction band edge has been shifted up, as obtained from a HSE calculation.

We studied the impact of five different N defects on the electronic structure of GaAsN alloys: we calculate the

electronic states, formation energies, and charge transition levels. The set of studied defects includes N_{As}, As_{Ga}, As_{Ga}-N_{As} substitutional defects and $(N\text{-}N)_{As}$, $(N\text{-}As)_{As}$ split-interstitial complex defects. We find that the formation energy of the neutral As_{Ga} defect is lower than that of substitutional N_{As}. Meanwhile, the formation energy of neutral $(N\text{-}N)_{As}$ is higher than for all the other defects, while our results also indicate that the $(N\text{-}As)_{As}$ split interstitial is the dominant interstitial complex defect in the neutral state of dilute GaAsN alloys. These results are in agreement with recent experimental results obtained using Rutherford backscattering spectroscopy (RBS) and nuclear reaction analysis spectra with Monte Carlo simulations [16], and other reports for GaAsN and related dilute nitride alloys [19–23,56]. As a prediction, we find that the antisite As_{Ga} defect is the most favorable one in $GaAs_{1-x}N_x$. The RBS spectra measured in Ref. [16] suggested the possible presence of Ga interstitial and/or As antisite in the $GaAs_{1-x}N_x$ alloys.

For the supercell calculations, the band structures were unfolded. Although nitrogen is isoelectronic with arsenic, because of the large difference in size and electronegativity between N and As atoms, this causes the formation of quasilocalized electron states associated with the substitution of N atoms, which interact strongly with the GaAs conduction band, and leads to a substantial reduction of the band gap. We find that the largest changes in the band structure are produced by an isolated N atom in GaAs, which is resonant with the conduction band, exhibiting a strong hybridization between N and GaAs states. Deeper levels in the energy gap, for which the energy required to transfer an electron (or hole) towards the conduction (or valence) band exceeds the characteristic thermal energy (k_BT), are obtained with $(N\text{-}N)_{As}$ and $(N\text{-}As)_{As}$ split-interstitial defects. Our results agree with those given by the band anticrossing model, which is appropriate to describe the electronic structure of GaAsN in the dilute limit [36].

ACKNOWLEDGMENTS

C.I.V. and J.D.F. acknowledge support as Investigadores Científicos of CONICET (Argentina). J.D.Q.-F. thanks CONICET for support via a postdoctoral fellowship and acknowledges support of a PIP 0650 (CONICET) grant. C.I.V. acknowledges support from CONICET (PIP-2015-11220150100538CO) and ANPCyT (PICT-2012-1069) grants. The authors would like to thank Dr. Paulo V. C. Medeiros and his co-workers for their BANDUP code. We thank the Centro de Simulación Computacional p/Aplicaciones Tecnológicas (CSC-CONICET) for granting the use of computational resources which allowed us to perform much of the simulations included in this work.

[1] J. F. Geisz and D. J. Friedman, Semicond. Sci. Technol. **17**, 769 (2002).
[2] M. Fischer, D. Gollub, and A. Forchel, Jpn. J. Appl. Phys. **41**, 1162 (2002).
[3] J. S. Harris, Jr., Semicond. Sci. Technol. **17**, 880 (2002).
[4] S. R. Kurtz, A. A. Allerman, E. D. Jones, J. M. Gee, J. J. Banas, and B. E. Hammons, Appl. Phys. Lett. **74**, 729 (1999).
[5] E. P. O'Reilly, A. Lindsay, P. J. Klar, A. Polimeni, and M. Capizzi, Semicond. Sci. Technol. **24**, 033001 (2009).
[6] N. Q. Thinh, I. A. Buyanova, P. N. Hai, W. M. Chen, H. P. Xin, and C. W. Tu, Phys. Rev. B **63**, 033203 (2001).
[7] S. G. Spruytte, C. W. Coldren, J. S. Harris, W. Wampler, P. Krispin, K. Ploog, and M. C. Larson, J. Appl. Phys. **89**, 4401 (2001).
[8] T. Ahlgren, E. Vainonen-Ahlgren, J. Likonen, W. Li, and M. Pessa, Appl. Phys. Lett. **80**, 2314 (2002).
[9] W. Li, M. Pessa, T. Ahlgren, and J. Decker, Appl. Phys. Lett. **79**, 1094 (2001).
[10] S. B. Zhang and S.-H. Wei, Phys. Rev. Lett. **86**, 1789 (2001).
[11] P. Carrier, S.-H. Wei, S. B. Zhang, and S. Kurtz, Phys. Rev. B **71**, 165212 (2005).
[12] V. Virkkala, V. Havu, F. Tuomisto, and M. J. Puska, Phys. Rev. B **85**, 085134 (2012).
[13] L. Ivanova, H. Eisele, M. P. Vaughan, P. Ebert, A. Lenz, R. Timm, O. Schumann, L. Geelhaar, M. Dähne, S. Fahy, H. Riechert, and E. P. O'Reilly, Phys. Rev. B **82**, 161201 (2010).
[14] J.-N. Beaudry, R. A. Masut, P. Desjardins, P. Wei, M. Chicoine, G. Bentoumi, R. Leonelli, F. Schiettekatte, and S. Guillon, J. Vac. Sci. Technol. A **22**, 771 (2004).
[15] M. Reason, H. A. McKay, W. Ye, S. Hanson, R. S. Goldman, and V. Rotberg, Appl. Phys. Lett. **85**, 1692 (2004).
[16] T. Jen, G. Vardar, Y. Q. Wang, and R. S. Goldman, Appl. Phys. Lett. **107**, 221904 (2015).
[17] K. Laaksonen, H.-P. Komsa, T. T. Rantala, and R. M. Nieminen, J. Phys.: Condens. Matter **20**, 235231 (2008).
[18] J. Occena, T. Jen, E. E. Rizzi, T. M. Johnson, J. Horwath, Y. Q. Wang, and R. S. Goldman, Appl. Phys. Lett. **110**, 242102 (2017).
[19] F. Ishikawa, S. Fuyuno, K. Higashi, M. Kondow, M. Machida, H. Oji, J.-Y. Son, A. Trampert, K. Umeno, Y. Furukawa, and A. Wakahara, Appl. Phys. Lett. **98**, 121915 (2011).
[20] K. M. Kim, W.-B. Kim, D. Krishnamurthy, J. H. Ryu, S. Hasegawa, and H. Asahi, J. Cryst. Growth **368**, 35 (2013).
[21] J. Chen, G. Ciatto, M. Le Du, J.-C. Harmand, and F. Glas, Phys. Rev. B **82**, 125303 (2010).
[22] H. P. Nair, A. M. Crook, K. M. Yu, and S. R. Bank, Appl. Phys. Lett. **100**, 021103 (2012).
[23] H. T. Pham, S. F. Yoon, K. H. Tan, and D. Boning, Appl. Phys. Lett. **90**, 092115 (2007).
[24] L.-W. Wang, Appl. Phys. Lett. **78**, 1565 (2001).
[25] B. K. Agrawal, S. Agrawal, P. S. Yadav, and S. Kumar, J. Phys.: Condens. Matter **9**, 1763 (1997).
[26] T. Mattila, S.-H. Wei, and A. Zunger, Phys. Rev. B **60**, R11245 (1999).
[27] P. R. C. Kent and A. Zunger, Phys. Rev. B **64**, 115208 (2001).
[28] M. Gladysiewicz, R. Kudrawiec, J. M. Miloszewski, P. Weetman, J. Misiewicz, and M. S. Wartak, J. Appl. Phys. **113**, 063514 (2013).
[29] A. Lindsay and E. O'Reilly, Solid State Commun. **112**, 443 (1999).
[30] A. Lindsay and E. O'Reilly, Solid State Commun. **118**, 313 (2001).

[31] A. Wadehra, J. W. Nicklas, and J. W. Wilkins, Appl. Phys. Lett. **97**, 092119 (2010).
[32] C. Freysoldt, B. Lange, J. Neugebauer, Q. Yan, J. L. Lyons, A. Janotti, and C. G. Van de Walle, Phys. Rev. B **93**, 165206 (2016).
[33] A. Janotti, S. B. Zhang, S.-H. Wei, and C. G. Van de Walle, Phys. Rev. Lett. **89**, 086403 (2002).
[34] S. M., M. R.H., H. M., T. D., and H. M., Phys. Status Solidi C **6**, 2652 (2009).
[35] S. L. Tan, W. M. Soong, J. E. Green, M. J. Steer, S. Zhang, L. J. J. Tan, J. S. Ng, I. P. Marko, S. J. Sweeney, A. R. Adams, J. Allam, and J. P. R. David, Appl. Phys. Lett. **103**, 102101 (2013).
[36] J. Wu, W. Shan, and W. Walukiewicz, Semicond. Sci. Technol. **17**, 860 (2002).
[37] C. G. V. de Walle and J. Neugebauer, J. Appl. Phys. **95**, 3851 (2004).
[38] C. Freysoldt, B. Grabowski, T. Hickel, J. Neugebauer, G. Kresse, A. Janotti, and C. G. Van de Walle, Rev. Mod. Phys. **86**, 253 (2014).
[39] T. Mattila and A. Zunger, Phys. Rev. B **58**, 1367 (1998).
[40] J. P. Perdew, K. Burke, and M. Ernzerhof, Phys. Rev. Lett. **77**, 3865 (1996).
[41] J. P. Perdew, K. Burke, and M. Ernzerhof, Phys. Rev. Lett. **78**, 1396 (1997).
[42] J. Heyd, G. E. Scuseria, and M. Ernzerhof, J. Chem. Phys. **118**, 8207 (2003).
[43] J. Heyd, G. E. Scuseria, and M. Ernzerhof, J. Chem. Phys. **124**, 219906 (2006).
[44] G. Kresse and J. Furthmüller, Phys. Rev. B **54**, 11169 (1996).
[45] D. Colleoni and A. Pasquarello, Phys. Rev. B **93**, 125208 (2016).
[46] P. V. C. Medeiros, S. Stafström, and J. Björk, Phys. Rev. B **89**, 041407 (2014).
[47] P. V. C. Medeiros, S. S. Tsirkin, S. Stafström, and J. Björk, Phys. Rev. B **91**, 041116 (2015).
[48] A. D. Becke and E. R. Johnson, J. Chem. Phys. **124**, 221101 (2006).
[49] F. Tran and P. Blaha, Phys. Rev. Lett. **102**, 226401 (2009).
[50] K. Momma and F. Izumi, J. Appl. Crystallogr. **44**, 1272 (2011).
[51] W. Orellana and A. C. Ferraz, Appl. Phys. Lett. **78**, 1231 (2001).
[52] R. Chtourou, F. Bousbih, S. B. Bouzid, F. F. Charfi, J. C. Harmand, G. Ungaro, and L. Largeau, Appl. Phys. Lett. **80**, 2075 (2002).
[53] J. E. Lowther, S. K. Estreicher, and H. Temkin, Appl. Phys. Lett. **79**, 200 (2001).
[54] W. Shan, W. Walukiewicz, J. W. Ager, E. E. Haller, J. F. Geisz, D. J. Friedman, J. M. Olson, and S. R. Kurtz, Phys. Rev. Lett. **82**, 1221 (1999).
[55] E. P. O'Reilly, A. Lindsay, and S. Fahy, J. Phys.: Condens. Matter **16**, S3257 (2004).
[56] J. Buckeridge, D. O. Scanlon, T. D. Veal, M. J. Ashwin, A. Walsh, and C. R. A. Catlow, Phys. Rev. B **89**, 014107 (2014).